Structural transition, electrical and magnetic properties of the B-site Co doped $Sr_{14}Cu_{24}O_{41}$ compounds

2009 J. Phys.: Condens. Matter 21 075601

(http://iopscience.iop.org/0953-8984/21/7/075601)

J. Phys.: Condens. Matter **21** (2009) 075601 (10pp) doi:10.1088/0953-8984/21/7/075601

Structural transition, electrical and magnetic properties of the B-site Co doped $Sr_{14}Cu_{24}O_{41}$ compounds

Jun Wang[1,2], **Ying Lin**[1], **Huamin Zou**[1,2,4], **Shizhou Pu**[1,2] and **Jing Shi**[1,3]

[1] Key Laboratory of Acoustic and Photonic Materials and Devices of the Ministry of Education, Department of Physics, Wuhan University, Wuhan 430072, People's Republic of China
[2] Center for Electron Microscopy, Wuhan University, Wuhan 430072, People's Republic of China
[3] International Center for Material Physics, Chinese Academies of Science, Shenyang, 110015, People's Republic of China

E-mail: hmzou@whu.edu.cn

Received 2 September 2008, in final form 18 December 2008
Published 13 January 2009
Online at stacks.iop.org/JPhysCM/21/075601

Abstract

The effect of Co substitution for Cu on the structure and physical properties of $Sr_{14}(Cu_{1-x}Co_x)_{24}O_{41}$ compounds was studied by analyzing the selected-area electron diffraction and convergent-beam electron diffraction patterns, and by measuring the magnetic susceptibility, the electrical resistivity and Raman spectra. It is found that the space group of the CuO_2 chain is changed from *Amma* to *Ammm* upon Co doping, but the structure of the Cu_2O_3 ladder remains unchanged. This indicates that the displacement between two neighboring CuO_2 chains has disappeared due to Co doping. Once a small amount of Co ions are doped into the compound, exceptional changes in the Weiss temperature and in the number of dimers occur. The remarkable increase in the absolute value of the Weiss temperature indicates that the antiferromagnetic interaction in CuO_2 chains becomes very strong due to Co doping. The increase in the Curie coefficient and the number of dimers implies that the Co doping causes Zhang–Rice singlets in the chains to be decoupled into free spins Cu^{2+} and holes. Then, the free spins Cu^{2+} are coupled into dimers, and the holes transfer from chains to ladders, which causes the resistivity to decrease when the Co dopant concentration is low ($x < 0.10$). When the Co dopant concentration is high ($x > 0.10$), some Co ions are directly substituted for the Cu ions in the ladders, which results in an increase in resistivity with increasing Co dopant content.

(Some figures in this article are in colour only in the electronic version)

1. Introduction

The quasi-one-dimensional spin 1/2 ladder compound $Sr_{14}Cu_{24}O_{41}$ has attracted much attention since it was first reported [1]. This compound has a unique crystal structure and exhibits abundant physical phenomena, such as sliding density waves [2], crystallization of charge holes [3], and the existence of superconductivity and a metal–insulator transition in the highly Ca doped compound [4].

[4] Author to whom any correspondence should be addressed.

The incommensurate composite compound $Sr_{14}Cu_{24}O_{41}$ possesses a layered structure of two alternating substructures, shown in figure 1: a two-leg Cu_2O_3 ladder sandwiched by Sr layers and an edge-sharing CuO_2 chain, which have different $\boldsymbol{c}$ axis lengths, $\boldsymbol{c}_L$ and $\boldsymbol{c}_C$ [4]. The spins in the Cu_2O_3 ladder are strongly antiferromagnetically coupled by nearly 180° Cu–O–Cu bonds. The space group of the substructure of the Cu_2O_3 ladder is *Fmmm*, while the space group of the CuO_2 chain substructure is *Amma*, in which Cu ions are coupled by nearly 90° Cu–O–Cu bonds along the $\boldsymbol{c}$ direction. The

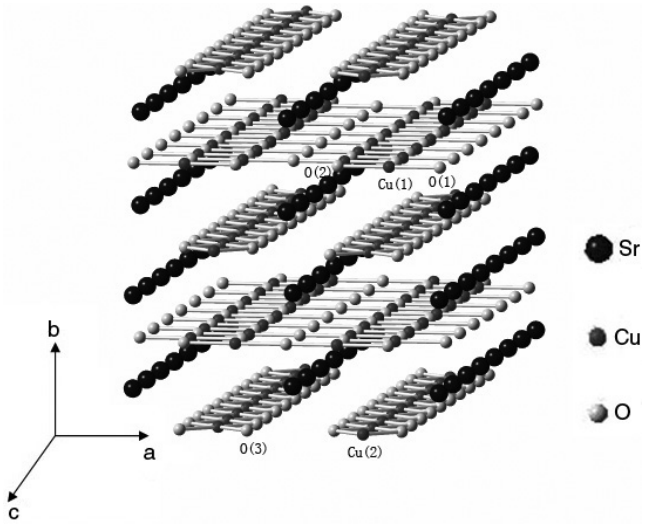

Figure 1. Incommensurately modulated structure of $Sr_{14}Cu_{24}O_{41}$. Two different Cu sites are illustrated.

ratio c_L:c_c is nearly $\sqrt{2}$:1. A significant feature of this kind of compound is that the average valence of Cu is +2.25, which implies that six holes per formula unit (f.u.) are already doped. It has been demonstrated that most holes are located in the CuO_2 chains [5]. Like for the high T_c superconductors, due to the strong Hubbard correlation of the 3d electrons of the Cu^{2+}, the holes are mainly located near the oxygen, and are coupled with the nearby Cu^{2+} ions to form Zhang–Rice singlets [6, 7]. The temperature dependence of the magnetic susceptibility χ shows a characteristic decrease below 80 K, which is considered as the contribution of spin dimers which are formed by the Cu^{2+} ion coupling across the Cu^{3+} with next-nearest-neighbor Cu^{2+} in the chains [8, 9].

Up to now, studies of the doping effect of $Sr_{14}Cu_{24}O_{41}$ have mainly focused on the substitution for Sr ions. For the Ca doped compound, $Sr_{14-x}Ca_xCu_{24}O_{41}$, the space group of the Cu_2O_3 ladder substructure is still $Fmmm$, while the space group of the CuO_2 chain substructure is changed from $Amma$ to $Fmmm$ [1]. In the meantime, due to doping of Ca ions the holes transfer from the chain to the ladder, which induces a decrease in electrical resistivity [5]. The susceptibility measurement for the $Sr_{14-x}Ca_xCu_{24}O_{41}$ shows that there is a nonmagnetic ground state with a gap of 120–130 K at about 80 K in the chain [8, 10]. NMR/NQR study shows that the spin gap of the ladder decreases with Ca substitution, but the spin gap for the chain is nearly independent of the substitution of Ca [11].

The structures and physical properties of the compounds in which Cu ions are substituted have been reported in a few literature entries. Lin *et al* [12] studied the effects of substitution of Cu by nonmagnetic Zn, Al and Ga ions. According to crystallography, as shown in figure 1, there is only one type of position for Sr, but there are two types of position for Cu: one in the CuO_2 chain, and another in the Cu_2O_3 ladder. The key point for the investigation of B-site doping is to determine at which positions the doping ions locate. The substitution for the Cu in different substructures, Cu_2O_3 ladders or CuO_2 chains, should result in different properties of the compound. However, the influence of doping on the substructure was not investigated in previous reports [12–14]. In the present paper, the structure and physical properties of the Co doped compounds are systematically studied. Transmission electron microscopy studies show that a new structural transition on the chain takes place after Co doping. Meanwhile, the temperature dependences of the static magnetic susceptibility, electrical resistivity, and Raman spectra for a series of $Sr_{14}(Cu_{1-x}Co_x)_{24}O_{41}$ compounds are measured. Then, the relation between the structural and physical properties of Co substituted compounds is discussed.

2. Experiments

Polycrystalline samples of $Sr_{14}(Cu_{1-x}Co_x)_{24}O_{41}$ were prepared by the standard solid-state reaction method. The starting powder materials of $SrCO_3$, CuO and Co_2O_3 with purities higher than 99.9% were mixed uniformly by ball milling, and then heated at 900 °C in air several times with intermediate grindings until the impurity phases were undetectable. The reacted samples were then pulverized, pressed into pellets and sintered for 24 h at 930 °C in air.

To measure the valence state of the Co ion in $Sr_{14}(Cu_{1-x}Co_x)_{24}O_{41}$ compounds, x-ray photoelectron spectroscopy (XPS) experiments were performed with an XSAM-800 (Kratos LTD). The XPS results show that the valence of the Co ion is +3 for every sample. Structure determination was carried out by selected-area electron diffraction and convergent-beam electron diffraction (CBED) techniques using a JEOL JEM2010 (HT) microscope operated at an accelerating voltage of 200 kV at room temperature. The temperature dependence of the static magnetic susceptibility was measured with a PPMS (Physical Property Measurement System, Quantum Design) from 10 to 300 K under a magnetic field of 1 T. Electrical resistivity measurements were carried out by the standard four-probe method. Raman spectrum measurements were performed in a backscattering configuration using an RM1000 (Renishaw LTD). All the spectra were excited with the 514.5 nm line of an Ar laser, and the scattered light was detected with a liquid-nitrogen-cooled CCD camera.

3. Results and discussion

3.1. Structural transition with the Co doping

Figure 2(a) shows the [010] zone axis electron diffraction pattern (EDP) of the undoped sample $Sr_{14}Cu_{24}O_{41}$. The main reflections are assigned by the superimposition of two sets of orthorhombic reciprocal lattices corresponding to the two subsystems: Cu_2O_3 ladders and CuO_2 chains. The real lattices of the two subsystems have approximately the common $\boldsymbol{a}$ ($a \approx$ 1.146 nm) and $\boldsymbol{b}$ ($b \approx$ 1.336 nm) dimensions, but different $\boldsymbol{c}$ dimensions ($c_L \approx$ 0.393 nm, $c_C \approx$ 0.275 nm). As given in figure 2(b), the intensity profile along the row of spots $(h02)_C$ in figure 2(a) shows clearly the intensities of each of the spots. It is seen from the profile that the $(102)_C$ spot is the brightest

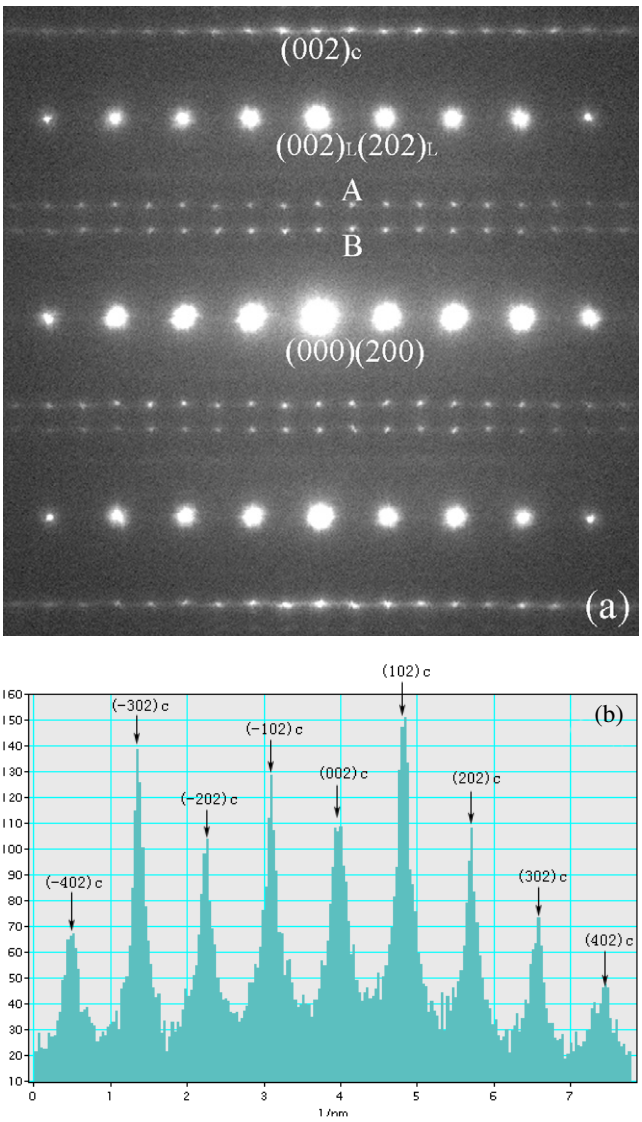

Figure 2. (a) [010] zone axis EDP of the undoped $Sr_{14}Cu_{24}O_{41}$. (b) The intensity profile along the $(h02)_C$ direction, in which the intensities of $(h02)_C$ spots with h = odd are strong.

spot in this row, and the intensities of the other $(h02)_C$ spots with h = odd are also higher than the spots with h = even. The theoretical calculation in the kinematical approximation gives the same results. The weak spots between the rows of $(h00)$ and $(h02)_L$ spots result from the double-diffraction effect of the two subsystems. For example, spot A can be produced by $(004)_L + (10\bar{2})_C$, spot B by $(00\bar{2})_L + (102)_C$. The diffraction streaks observed in EDP are due to the initial phase disorder in the structure [15].

It was also found that the $(h02)_C$ spots with h = odd remain stronger than the spots with h = even in the [010] zone axis diffraction patterns of Zn and Ni doped compounds [16]. This means that the substitutions of Cu ions either by nonmagnetic Zn^{2+} ions or by weak magnetic Ni^{2+} ions do not induce any changes in the structure of the compound. However, the substitution of strong magnetic Co^{3+} for Cu ions, even at a low level such as $x = 0.02$, results in a significant change in the [010] diffraction pattern. As shown in figure 4(a), the $(h02)_C$ spots with h = odd disappear, which can be seen more clearly from the double-diffraction spots. This indicates that a certain structural change happens upon Co^{3+} doping.

The CBED method was used to determine the symmetry of the composite crystal $Sr_{14}(Cu_{1-x}Co_x)_{24}O_{41}$ which contains both ladder and chain substructures. It is found that the structural transition occurs when a small amount of Co ions are doped into the compound, and the structure does not change further if more Co ions are doped in. Figures 3(a), 4(a) and 5(a) show the [001], [010] and [100] zone axis electron diffraction patterns of $Sr_{14}(Cu_{0.82}Co_{0.18})_{24}O_{41}$, respectively. It is found that both the Cu_2O_3 ladder and CuO_2 chain substructures belong to the orthorhombic crystal system. The whole CBED pattern taken from the [001] zone axis is shown in figure 3(b). It is seen that there exist a twofold rotation axis parallel to the [001] direction and mirror planes parallel not only to the (100) plane but also to the (010) plane. Hence, the whole pattern has $2mm$ symmetry. Similar investigations for the [010] and [100] zone axis CBED whole patterns, as illustrated in figures 4(b) and 5(b) respectively, show that the two whole patterns also have $2mm$ symmetry. That is, the CBED observations show that there are three mirror planes respectively perpendicular to the [100], [010] and [001] twofold rotation axes. Hence, the point group determined by the CBED patterns is mmm (or $\frac{2}{m}\frac{2}{m}\frac{2}{m}$ to give the full Hermann–Mauguin symbol) [17]. It is known that the symmetry of the composite crystal cannot be higher than the symmetries of the two subsystems, and the highest point symmetry of the orthorhombic system is mmm. Therefore, the point groups of both subsystems are determined as mmm.

Among the [100], [010] and [001] diffraction patterns of the chain substructure shown in figures 3(a), 4(a) and 5(a) respectively, the centered spot in a rectangle appears only in the [100] diffraction pattern. This shows that the lattice of chain substructure is a side centered orthorhombic lattice. Comparing figure 4(a) with figure 2(a), it is found that the spots $(h02)_C$ with h = odd disappear for the Co doped sample. In fact, in the case of the Co doped sample with the side centered orthorhombic lattice, the indexes of spots $(200)_C$, $(202)_C \cdots$ in the [010] pattern, as shown in figure 4(a), which were originally assigned for the undoped sample, can be reassigned as $(100)_C$, $(102)_C \cdots$ respectively. Thus the reflection conditions obtained from [100], [010] and [001] diffraction patterns are: for $0kl$ reflections, $k+l$ = even, which is a special case of the general condition for the A side centered lattice $k + l$ = even for hkl reflections; for $h0l$ reflections, l = even; for $hk0$ reflections, k = even. Finally, according to table 3.2 of [18], the space group of the chain substructure for the Co doped sample is obtained as $Ammm$ (#65). Here, the length of the $\boldsymbol{a}$ axis for the Co doped sample is half of that for the undoped sample. However there are no changes in the diffraction patters of the ladder substructure after Co doping, so the space group of the ladder substructure remains $Fmmm$ [1].

According to the data of McCarron *et al* [1], the CuO_2 chain substructure of the undoped $Sr_{14}Cu_{24}O_{41}$ has space group $Amma$ (#63), and Cu and O atoms occupy 4c positions with fractional coordinates (1/4, 0, 0.085) and 8f positions

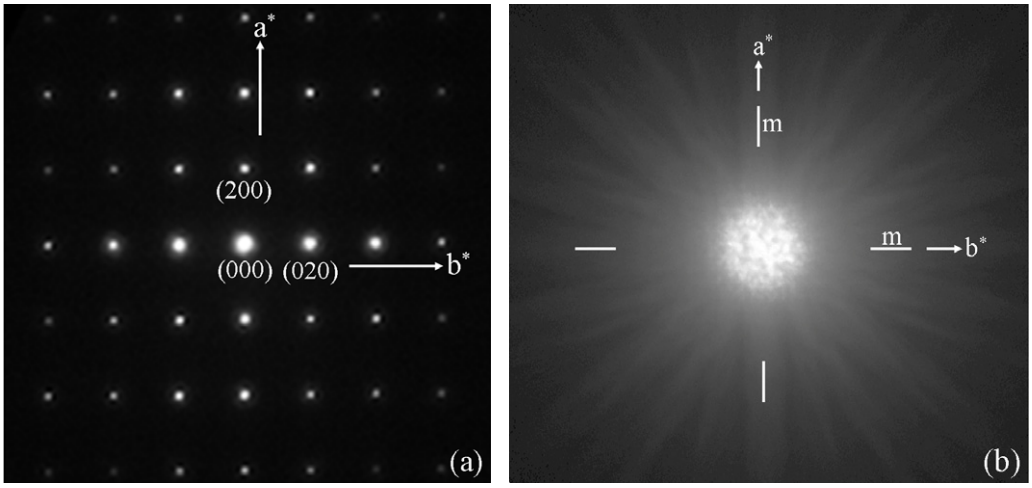

Figure 3. (a) [001] zone axis EDP of $Sr_{14}(Cu_{0.82}Co_{0.18})_{24}O_{41}$. (b) [001] zone axis CBED whole pattern of $Sr_{14}(Cu_{0.82}Co_{0.18})_{24}O_{41}$ showing the symmetry $2mm$.

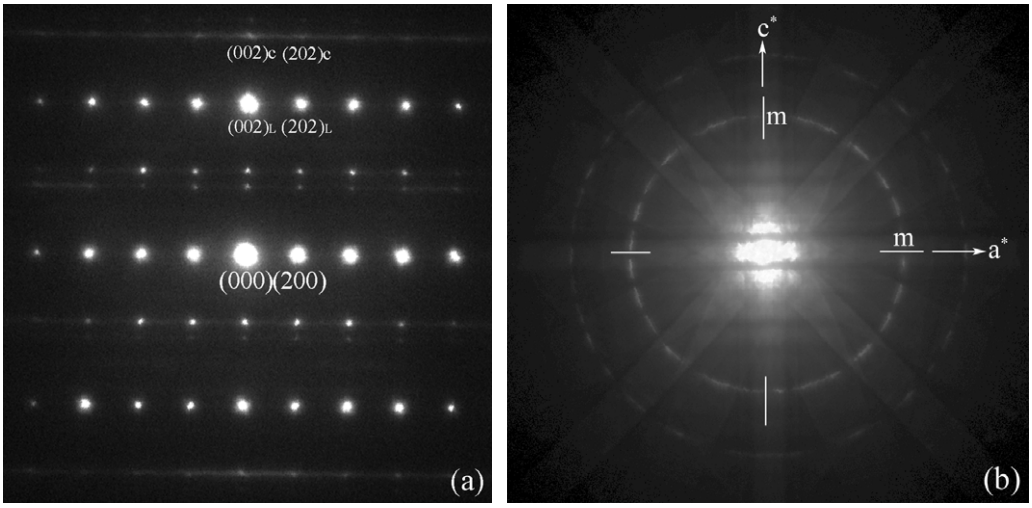

Figure 4. (a) [010] zone axis EDP of $Sr_{14}(Cu_{0.82}Co_{0.18})_{24}O_{41}$. (b) [010] zone axis CBED whole pattern of $Sr_{14}(Cu_{0.82}Co_{0.18})_{24}O_{41}$ showing symmetry $2mm$.

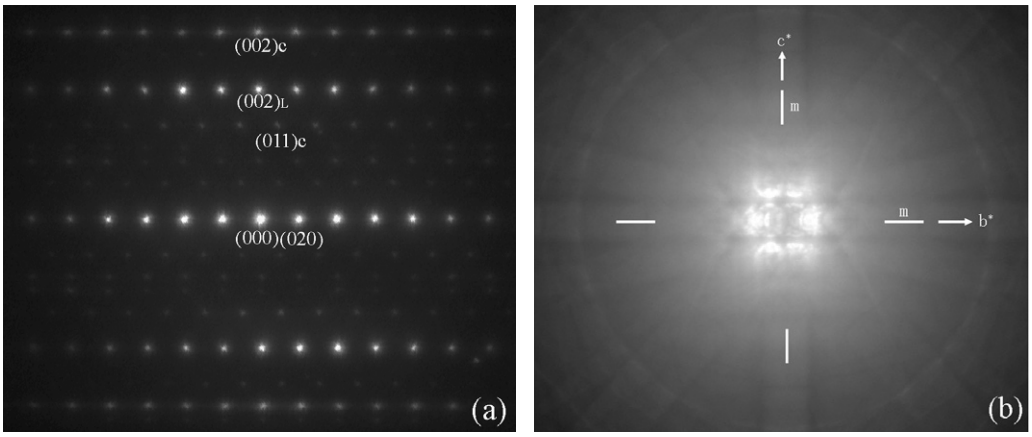

Figure 5. (a) [100] zone axis EDP of $Sr_{14}(Cu_{0.82}Co_{0.18})_{24}O_{41}$. (b) [100] zone axis CBED whole pattern of $Sr_{14}(Cu_{0.82}Co_{0.18})_{24}O_{41}$ showing symmetry $2mm$.

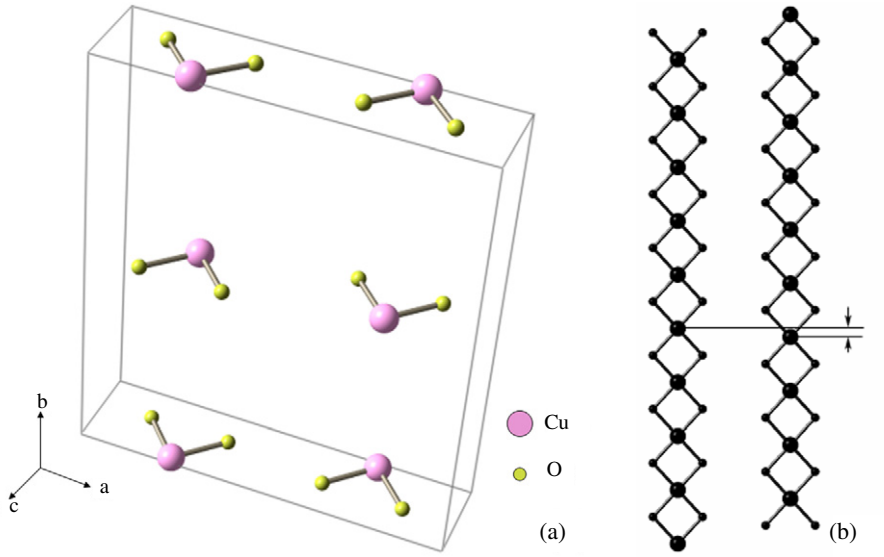

Figure 6. (a) Three-dimensional sketch of the unit cell of the CuO_2 chain substructure in $Sr_{14}Cu_{24}O_{41}$. (b) Relative positions of two neighboring CuO_2 chains of $Sr_{14}Cu_{24}O_{41}$ along the $\boldsymbol{c}$ direction, in which the displacement between two neighboring CuO_2 chains is indicated.

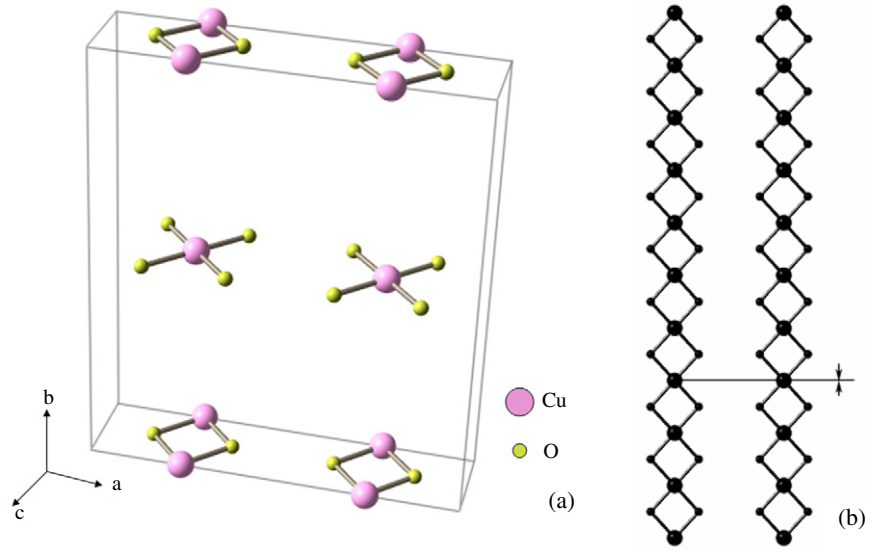

Figure 7. (a) Three-dimensional sketch of the unit cell of the CuO_2 chain substructure in $Sr_{14}(Cu_{1-x}Co_x)_{24}O_{41}$. In order to facilitate comparison with figure 6, the edge length in the $\boldsymbol{a}$ direction here is double the real length of the $\boldsymbol{a}$ axis of the unit cell of the chain substructure of the Co doped sample. (b) Relative positions of two neighboring CuO_2 chains of $Sr_{14}(Cu_{1-x}Co_x)_{24}O_{41}$ along the $\boldsymbol{c}$ direction, in which the displacement between two neighboring CuO_2 chains disappears.

with coordinates (0.360, 0, 0.588), respectively, as shown in figure 6. It is seen from figure 6 that, for the pure $Sr_{14}Cu_{24}O_{41}$, there is a displacement between the two neighboring CuO_2 chains. The site symmetries of 4c and 8f in space group *Amma* are *mm*2 and *.m.* respectively. To satisfy the requirements of the space group symmetry, the Cu and O atoms may shift a little bit (0.085) along the $\boldsymbol{c}$ axis to the positions with site symmetries *mmm* and 2*mm*, i.e., 2d and 4l positions of space group *Ammm*, respectively. Figure 7 shows the CuO_2 chain substructure of the Co doped sample in which the positions of Cu and O are (0.5, 0, 0) and (0.72, 0, 0.5) respectively. Here, the fact that the length of the $\boldsymbol{a}$ axis for the Co doped sample is a half of that for the undoped sample has been taken into account. Besides, this is evidence that Cu ions in the CuO_2 chains are substituted by the doping Co ions.

3.2. Magnetic susceptibility

The temperature dependence of the total magnetic susceptibility can be described as the sum of a temperature independent term χ_{const}, a Curie–Weiss term χ_{CW}, a ladder term χ_{ladder}, and a dimer term χ_{dimer} in units of emu/Cu mol [8, 19]:

$$\chi_{total} = \chi_{const} + \chi_{CW} + \chi_{ladder} + \chi_{dimer}. \quad (1)$$

Here, the temperature independent term χ_{const}, which represents the sum of the core diamagnetic term and the

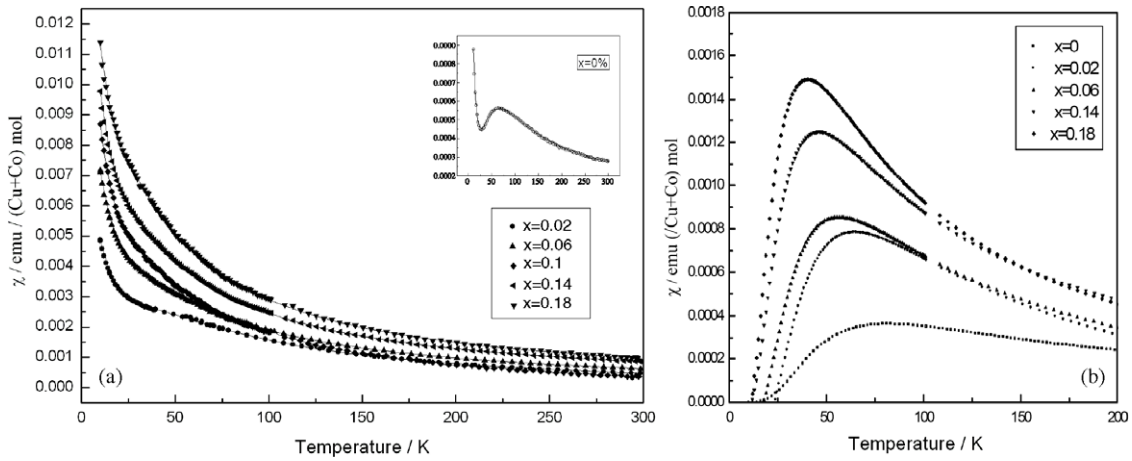

Figure 8. (a) The measured temperature dependence of the magnetic susceptibility of $Sr_{14}(Cu_{1-x}Co_x)_{24}O_{41}$ ($x = 0$, 0.02, 0.06, 0.10, 0.14, 0.18). The experimental data (open circles) and the fitting curve (solid line) for the undoped sample ($x = 0$) are shown in the inset. (b) The temperature dependence of χ_{dimer}, which is obtained by subtracting the Curie–Weiss term from the measured susceptibility.

Van Vleck paramagnetic term, is very small and can be neglected [20]. Because the term for the Cu_2O_3 ladder has a very large gap of 400 K [21], χ_{ladder} can be ignored in the range of observation temperature. It is considered that χ_{CW} comes from the contribution of the free spins which do not participate in the dimerized state in the CuO_2 chain. Below 20 K, χ_{CW} can be well fitted with the Curie–Weiss law:

$$\chi_{CW} = C/(T - \Theta). \tag{2}$$

Here, C is the Curie coefficient. Unlike for the nonmagnetic ion doping, not only the free spins Cu^{2+}, but also the magnetic Co^{3+} ions contribute to the χ_{CW} term. So the unit of the Curie coefficient becomes emu K/(Cu + Co) mol. Assuming that Co^{3+} ions do not participate in the formation of dimers, χ_{dimer} can be described as

$$\chi_{dimer} = 2N_D(N_A/24)g^2\mu_B^2/\{k_BT[3 + \exp(J_D/k_BT)]\}. \tag{3}$$

Here, N_A is Avogadro's number, the Landé g-factor is 2.2 [21], k_B and Θ are the Boltzmann constant and Weiss temperature, respectively, while J_D is the dimer coupling constant, and N_D is the number of dimers per formula unit (f.u.). Figure 8(a) shows the temperature dependence of the susceptibility of the Co doped samples. The experimental data and the fitting curve for the undoped sample are shown in the inset of figure 8(a). It is seen that the curve fits the experimental data very well. More details about the fitting procedure can be found in [22].

By fitting the χ–T curve for every sample with the equations (1)–(3), we obtained the values of C, Θ, N_D and J_D as shown in table 1. The temperature dependence of χ_{dimer} is shown in figure 8(b). Remarkable changes in the magnetic parameters of Co^{3+} doped samples can be seen even if a small amount of Cu ions are substituted by Co^{3+}. With increase in Co content, the broad peak, which locates around 80 K for the undoped sample, becomes stronger and shifts to lower temperatures. The Curie coefficient C for the sample with $x = 0.02$ is more than ten times larger than that of the undoped sample. Afterward, the Curie coefficient C increases much more slowly as the Co content further increases. Similarly, the Weiss temperature Θ jumps from -0.52 to -6.52 as a small amount of Co ions ($x = 0.02$) are doped, while it changes very slowly when more Co ions are doped. The Θ remains negative, while the absolute value increases in a similar way to the Curie coefficient. The number of dimers in CuO_2 chains per f.u. increases abruptly from 1.56 to 2.8 once 2% Cu ions are substituted by Co^{3+}, while it increases slowly for doping in more Co^{3+}. The dimer coupling constant J_D decreases as the Co content increases. This means that the intradimer coupling decreases when more magnetic Co^{3+} ions are doped into the sample. Also the absolute value of the increment of J_D between the pure sample and the sample with $x = 0.02$ is the biggest, comparing with the others.

Table 1. Fitting results with equations (1)–(3) for $Sr_{14}(Cu_{1-x}Co_x)_{24}O_{41}$. The values of the Curie coefficient C, Weiss temperature Θ, number of dimers per f.u. N_D, and dimer coupling constant J_D are listed.

Dopant level, x	C (emu K/(Cu + Co) mol)	Θ (K)	N_D	J_D (K)
0.00	0.0077 ± 0.0102	-0.52 ± 0.21	1.56 ± 0.01	131 ± 0.4
0.02	0.0992 ± 0.0118	-6.52 ± 0.46	2.80 ± 0.01	104 ± 0.3
0.06	0.130 ± 0.0086	-7.86 ± 0.24	2.90 ± 0.01	91 ± 0.9
0.10	0.147 ± 0.0028	-6.01 ± 0.32	2.80 ± 0.01	76 ± 0.5
0.14	0.168 ± 0.0094	-7.12 ± 0.18	3.00 ± 0.01	74 ± 0.5
0.18	0.213 ± 0.0362	-8.83 ± 0.61	3.10 ± 0.01	65 ± 1.0

It is well known that there are three states of Cu ions in the CuO_2 chains: the first one is the free spin Cu^{2+} with spin $s = 1/2$; the second one is the nonmagnetic Zhang–Rice singlet which includes a Cu^{2+} spin located at the center of square of O atoms and a hole located near the oxygen atoms due to the large Hubbard correlation of 3d electrons of the Cu^{2+} [23]; the third one is the dimer which is formed by two nearby Cu^{2+} spins with one Zhang–Rice singlet in the middle, namely $\langle\uparrow\ 0\ \downarrow\rangle$. From table 1, the number of dimers in the undoped sample is 1.56. And the number of free spins Cu^{2+} in

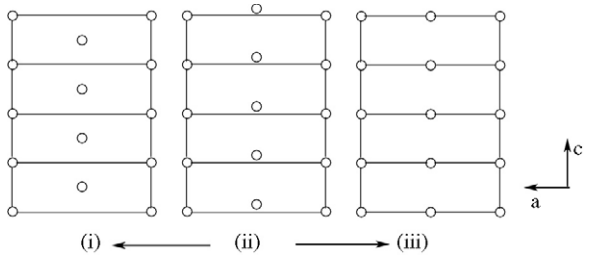

Figure 9. Three different CuO_2 chain substructures. Here the open circles represent the copper ions, and the oxygen ions are not shown.

the chain is 0.41 as calculated from the equation

$$C = N_F(N_A/24)g^2\mu_B^2 s(s+1)/3k_B, \quad (4)$$

where C is the Curie coefficient, N_F is the number of free spins Cu^{2+} or Co^{3+} in the chain per formula unit.

As mentioned before, the Curie coefficient of the slightly Co doped sample ($x = 0.02$) is more than ten times larger than that of the undoped one. It is known that $s = 1/2$ for Cu^{2+} ($3d^9$) and $s = 2$ for the high spin state of Co^{3+} ($3d^6$). If Cu^{2+} ions are substituted by Co^{3+}, the value of s in equation (4) must be changed from 1/2 (for Cu^{2+}) to 2 (for Co^{3+}); thus the contribution of Co^{3+} to the Curie term is eight times as large as that of Cu^{2+}. This must be one of the reasons for the rapid increase in Curie coefficient and the absolute value of the Weiss temperature of the slightly Co doped compound. Also this may be further evidence that Cu ions in CuO_2 chains are substituted by Co^{3+} ions, in addition to the structural transition of the chain.

Besides, if the Curie term comes only from the contribution of free spins Cu^{2+}, the number of free spins Cu^{2+} within the chain can be calculated by using the values of the Curie coefficient in table 1 and the relationship that a Curie coefficient of 0.0077 corresponds to 0.41 Cu^{2+}/f.u. The sum of the number of free spins and the number of Cu^{2+} in dimers (two spins for each dimer) for all the doped samples is larger than 10, the total number of Cu sites per f.u. This is obviously impossible. The possible explanations for the rapid increase in Curie coefficient upon Co doping are: (1) the spins of Co^{3+} ions do make a direct contribution to the Curie coefficient; (2) the moment of Co^{3+} depends on its coordination, the spin state of Co^{3+} may be changed along with the coordination upon doping and the magnetic behavior is a strong function of the spin state; (3) upon Co doping, more adjacent Cu^{2+} ions are bridged by oxygen ions and form strongly antiferromagnetic dimers and trimers.

The rapid increase in the absolute value of the Weiss temperature may also be due to Co^{3+} having a temperature dependent moment due to the splitting of the d orbitals in non-cubic fields. Such a moment shows up as a non-zero Θ.

The assumption that Co^{3+} ions do not participate in the formation of dimers is reasonable. First, there is only one peak in the curve of magnetic susceptibility versus temperature as shown in figure 8(b). Since the core susceptibilities and spins of Co^{3+} and Cu^{2+} are different, if Co^{3+} were coupled with Cu^{2+} (or nearby Co^{3+}), the spin gap should be different from the Cu^{2+}–Cu^{2+} coupling and a new peak should be observed in figure 8(b) according to the alternating linear chain model of Hatfield [25, 26]. The phenomenon that the broad peak shifts to lower temperature with Co^{3+} doping is similar to that in the case of La^{3+} doping in which substitution of La^{3+} for Sr^{2+} can only make the holes decrease in the system, and make the dimers decoupled into free spins Cu^{2+} [24]. Second, if Co^{3+} participated in the formation of dimers, the number of dimers should increase more rapidly with Co doping amount. But it does not. Except that N_D increases by a large number when a small amount ($x = 0.02$) of Co is initially doped into the compound, the N_D increases very slowly with Co doping.

There is an interesting phenomenon relating the structure and the magnetic properties. Figure 9 shows three situations for the adjacent CuO_2 chains. Figure 9(i) shows two neighboring CuO_2 chains having 90° phase displacement. The relative displacement decreases from (i) to (ii); up to (iii) no displacement exists. As we known, there is a small displacement between two adjacent CuO_2 chains for the pure $Sr_{14}Cu_{24}O_{41}$ as shown in figure 9(ii). It is found that the CuO_2 chains can shift relatively along the c axis after doping with some ions since the interaction between the CuO_2 chains is very weak. For Ca^{2+} doping, the chain substructure changes from (ii) to (i) [1]. For Y^{3+} doping, the displacement increases with increase in the Y^{3+} content, while the chain substructure of $Sr_8Y_6Cu_{24}O_{41}$ also changes from (ii) to (i) [27]. Generally, as the substructure changes from (ii) to (i), the number of dimers in CuO_2 chains decreases [19, 26], no matter which kind of ion is doped in. However, as discussed in section 3.1, for Co^{3+} doping in our experiment, the CuO_2 chain substructure changes from (ii) to (iii), which has not been reported as far as we know; in the meantime the number of dimers increases, as shown in table 1 and figure 8(b), where the peak of susceptibility becomes higher with increase in Co content. In general, the number of dimers increases with decrease in the displacement between two neighboring CuO_2 chains, such as from (i) to (iii).

3.3. Electrical resistivity and hole distribution

The temperature dependence of the electrical resistivity for $Sr_{14}(Cu_{1-x}Co_x)_{24}O_{41}$ with $x = 0$, 0.02, 0.06, 0.10, 0.14, and 0.18 is shown in figure 10. As for the undoped sample, all the Co doped samples are semiconducting; no metal–insulator transition is observed. As the Co content x increases, the resistivity decreases firstly when x is less than 0.10, and then increases when x is larger than 0.10. It is noticed that the results of resistivity measurements in our experiment are different from those of Yoshimitsu *et al* [13]. The reason for this kind of difference might be that the valence of the Co ions in the experiment of Yoshimitsu *et al* [13] is +2, while it is +3 in our experiment according to the XPS measurements. Besides, the proportions of the doped Co ions distributed in ladders and in chains may be different. Investigation of $(Sr, A)_{14}Cu_{24}O_{41}$ (A = Ca, La) [28] showed that the Arrhenius plot $\ln\rho$–T^{-1} exhibits a bend at a temperature $T\rho$ which indicates a change in the conduction mechanism at $T\rho$. The Arrhenius plot $\ln\rho$–T^{-1} is shown for every sample of our

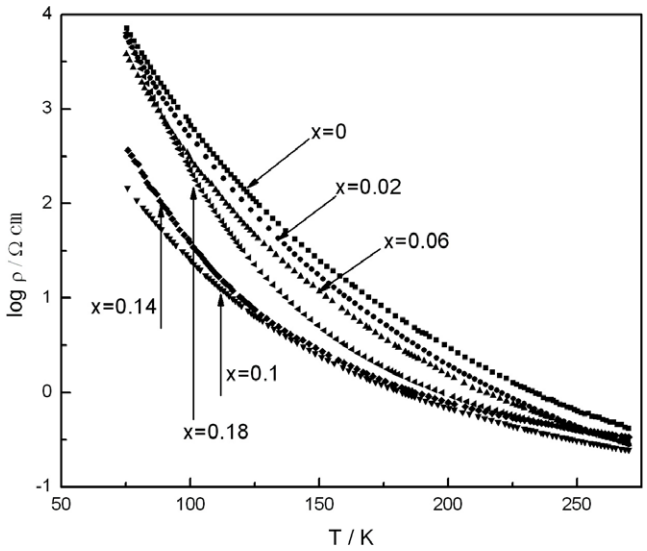

Figure 10. Temperature dependence of the resistivity for $Sr_{14}(Cu_{1-x}Co_x)_{24}O_{41}$.

experiment in figures 11(a) and (b). Table 2 shows the values of $T\rho$. When the Co content is small, e.g. $x = 0.02, 0.06$, the resistivity decreases with x, but $T\rho$ decreases very slightly, as shown in figure 11(a) and table 2. This is because some holes transfer from the chains to the ladders, which is similar to the case for $Sr_{14-x}Ca_xCu_{24}O_{41}$ [29]. When more Co ions are doped in, especially when $x > 0.10$, the resistivity increases with x, and the bend in the Arrhenius plot becomes unclear. This suggests that the conduction mechanism does not change for slightly Co doped samples, but it may be changed for highly Co doped samples.

As we know, the transport properties of the $Sr_{14}Cu_{24}O_{41}$ family compounds are mainly determined by the Cu_2O_3 ladder. The change in resistivity caused through substitution is due to

Table 2. The values of $T\rho$ for $Sr_{14}(Cu_{1-x}Co_x)_{24}O_{41}$.

Dopant level, x	$T\rho$ (K)
0.00	210
0.02	201
0.06	196
0.10	167
0.14	110
0.18	105

the redistribution of holes between CuO_2 chains and Cu_2O_3 ladders. When Ca is substituted for Sr, the holes transfer from chains to the ladders, which results in a decrease of the resistivity [30].

As shown previously, the Cu^{2+} ions in the chains are substituted by the doped Co^{3+} ions when the Co^{3+} content $x < 0.10$, and the Co^{3+} ions do not participate in the formation of dimers. For the sample with $x = 0.02$, the contribution of all the doped Co^{3+} ions to the Curie coefficient is only 0.0726 emu K/(Cu + Co) mol, based on the calculation with equation (4) using $N_F = 0.48$ and $s = 2$. Thus, the remainder of the Curie coefficient, 0.0266 (=0.0992 − 0.0726) emu K/(Cu + Co) mol, is the contribution of 1.42 free spins Cu^{2+} per formula unit, which is larger than 0.41, the number of free spins Cu^{2+} in the undoped sample. Meanwhile, the N_D increases from 1.56 to 2.8. In order to satisfy these conditions, some of the Zhang–Rice singlets in the chains should be decoupled into free spins Cu^{2+} and holes, and the holes are transferred from the chains to the ladders. Some of the decoupled Cu^{2+} free spins can be coupled with other Cu^{2+} and Zhang–Rice singlets to form dimers; the remainder contribute to the Curie–Weiss term as free spins, Cu^{2+}. Like for the case of the Ca doped compound $Sr_{14-x}Ca_xCu_{24}O_{41}$ [30], when $x < 0.10$ in the case of the Co doped compound, the resistivity decreases when the holes transfer from chains to the ladders, as shown in figures 10 and 11(a). Also, the conduction mechanism in this case is the

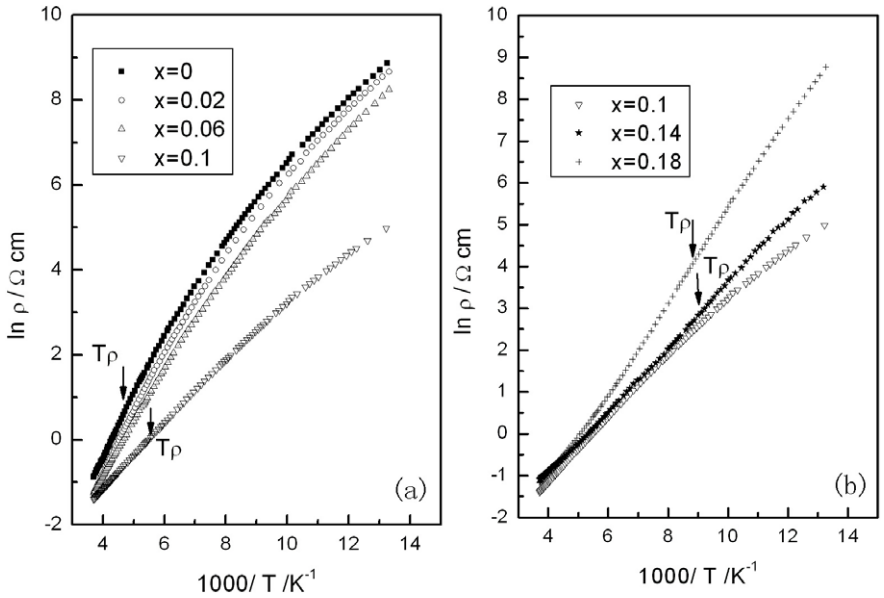

Figure 11. The Arrhenius plot ln ρ–T^{-1} for $Sr_{14}(Cu_{1-x}Co_x)_{24}O_{41}$. The values of the crossover temperature T_ρ shown in table 2 are determined as the peak temperatures of the $d(\ln \rho)/d(T^{-1}) \sim T$ plot.

same as that for the undoped compound, which is in accord with the experiment shown in figure 11(a).

When more Co ions are doped, especially when $x > 0.10$, the number of dimers increases very slowly as shown in table 1. At the same time, the Curie–Weiss term also increases. However, if all the Co^{3+} ions contribute to the Curie–Weiss term, the Curie coefficient should be larger than our experimental values. Therefore, when the Co content exceeds a certain value ($x > 0.10$), some Co ions must substitute for Cu ions in the ladders. The substitution of Co for Cu in the ladders may suppress the charge ordering in the Cu_2O_3 ladders proposed in [31], which leads to decrease of the resistivity and a change in conduction mechanism from that of the undoped sample. As mentioned before, although the substitution of Co^{3+} for Cu^{2+} will reduce the number of holes in the whole system, the holes are still transferred from the chains to the ladders when small amounts of Co^{3+} ions ($x < 0.1$) are substituted for Cu^{2+} ions. However, when the Co dopant concentration is larger, some Co^{3+} ions are directly substituted for Cu^{2+} in the ladders, which reduces the holes in the ladders. These two opposite processes lead to a maximum number of holes in the Cu_2O_3 ladders. Considering the suppression of charge ordering and the existence of the maximum number of holes in the ladders, the resistivity reaches its minimum when the Co dopant concentration $x = 0.1$ in our experiment. Then, as more and more Co^{3+} ions are substituted for the Cu^{2+} ions in the ladders, the number of holes in the ladders becomes smaller and smaller, which results in an increase in resistivity with Co dopant content when $x > 0.10$. With this assumption, the transport property shown in figures 11(a) and (b) can be explained. Besides, it is noticed that the absolute values of N_D and Θ for the sample with $x = 0.10$ are smaller than those for the samples with $x = 0.06$ and 0.14. The reason might be that for the sample with a total dopant content of 0.10, the number of Co ions effectively doped into CuO_2 chains may be less than that for the sample with $x = 0.06$ because some Co ions are directly doped into Cu_2O_3 ladders, and when the total dopant amount is larger than 0.10, e.g. 0.14, the Co^{3+} content in CuO_2 chains may increase too. And this phenomenon also indicates that for more Co doping, not only the Cu ions in CuO_2 chains, but also those in Cu_2O_3 ladders may be substituted by Co.

3.4. Raman spectra

Figure 12 shows the Raman spectra of $Sr_{14}(Cu_{1-x}Co_x)_{24}O_{41}$. The $(4A_g + 4B_{1g} + 3B_{2g} + B_{3g})$ modes are Raman allowed for the $Sr_{14}Cu_{24}O_{41}$ compound family [32–34]. The modes at 246, 301, 558 and 580 cm^{-1} are assigned to Sr, ladder-Cu(1), chain-O(3) and ladder-O(1), respectively [34]. The remarkable decrease in the intensity of the ladder-O(1) mode at 580 cm^{-1} with increase in the Co^{3+} content, as shown in figure 12, indicates that the holes are transferred from chains to the ladders, just like the similar decrease observed in $Sr_{14-x}Ca_xCu_{24}O_{41}$ [34] and other CuO_2-plane modes in the high T_c cuprates [35]. When the Co content is less than 0.10, the peak at 301 cm^{-1} does not shift with Co content change. However, when the Co content is larger than 0.10, the shift of the 301 cm^{-1} mode is 10 cm^{-1} for $x = 0.10$, and 15 cm^{-1} for $x = 0.14$, respectively, whereas the other frequency modes are nearly unchanged. This is the evidence that some Co^{3+} ions are substituted for the Cu^{2+} in the Cu_2O_3 ladders when the doped Co content $x > 0.10$. Since the atomic mass and ionic radius of Co^{3+} are smaller than those of Cu^{2+}, the average mass and ionic radius decrease with the doped Co content, and thus the frequency of the ladder-Cu(1) mode becomes higher. The results of the Raman experiment accord very well with the results of resistivity measurements as discussed above.

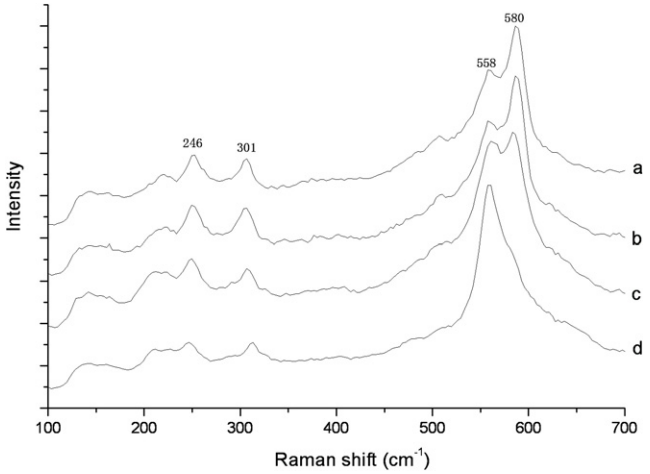

Figure 12. Unpolarized Raman spectra of $Sr_{14}(Cu_{1-x}Co_x)_{24}O_{41}$ polycrystalline samples: (a) $x = 0$; (b) $x = 0.02$; (c) $x = 0.10$; (d) $x = 0.14$. The peak of 301 cm^{-1} is shifted and the intensity of the 580 cm^{-1} peak decreases when the Co content is more than 0.10. This phenomenon can be seen more clearly for larger Co dopant concentration, such as $x = 0.14$, as shown in (d).

4. Conclusion

The TEM study reveals that, when magnetic Co ions are substituted for Cu ions in $Sr_{14}Cu_{24}O_{41}$ compound, the structure of the CuO_2 chain changes, but the structure of the Cu_2O_3 ladder remains unchanged. The space group of the CuO_2 chain changes from *Amma* to *Ammm* upon Co doping, which indicates that the relative displacement of two neighboring CuO_2 chains does not exist any longer.

The measurements of the magnetic susceptibility and the electrical resistivity show that the doped Co content has a strong influence on the magnetic and transport properties of $Sr_{14}(Cu_{1-x}Co_x)_{24}O_{41}$ compound. The exceptional increase in the absolute value of the Curie coefficient for slight Co doping is due to the larger spin of the free spins Co^{3+} in comparison with Cu^{2+}. The remarkable increase in the number of dimers may result from some Zhang–Rice singlets originally existing in the undoped sample being decoupled after Co doping, and some of the free spins Cu^{2+} from the decoupled Zhang–Rice singlets being coupled to the dimers; the remainder contribute to the Curie–Weiss term. For slight Co doping, the holes are transferred from chains to ladders, which causes the decrease in resistivity, while when the Co content x is larger than 0.10, the conduction mechanism is changed. Also, the resistivity

increases with the Co content when $x > 0.10$, which may be due to some of the Co ions being directly substituted for Cu in the ladder.

Raman spectra of the $Sr_{14}(Cu_{1-x}Co_x)_{24}O_{41}$ confirm that the holes are transferred from the chains to the ladders, the Co^{3+} ions are substituted for Cu^{2+} ions in the chains when $x < 0.10$, while some of the Co^{3+} ions are doped into the ladders when $x > 0.10$.

Acknowledgments

This work was supported financially by the National Natural Science Foundation of China (Nos 10674105 and 50471028).

References

[1] McCarron E M, Subramanian M A, Calabrese J C and Harlow R L 1988 *Mater. Res. Bull.* **23** 1355
[2] Blumberg G, Littlewood P, Gozar A, Dennis B S, Motoyama N, Eisaki H and Uehida S 2002 *Science* **297** 584
[3] Abbamonte P, Blumberg G, Rusydi A, Gozar A, Evans P G, Siegrist T, Venema L, Eisaki H, Isaacs E D and Sawatzky G A 2004 *Nature* **431** 1078
[4] Uehara M, Nagata T, Akimitsu J, Takahashi H, Mori N and Kinoshita K 1996 *J. Phys. Soc. Japan* **65** 2764
[5] Kato M, Shiota K and Koike Y 1996 *Physica* C **258** 284
[6] Nücker N, Merz M, Kuntscher C A, Gerhold S, Schuppler S, Neudert R, Golden M S, Fink J, Schild D, Stadler S, Chakarian V, Freeland J, Idzerda Y U, Conder K, Uehara M, Nagata T, Akimitsu J, Motoyama N, Eisaki H, Uchida S, Ammerahl U and Revcolevschi A 2000 *Phys. Rev.* B **62** 14384
[7] Zhang F C and Rice T M 1988 *Phys. Rev.* B **37** 3759
[8] Carter S A, Batlogg B, Cava R J, Krajewski J J, Peck J W F and Rice T M 1996 *Phys. Rev. Lett.* **77** 1378
[9] Eccleston R S, Uehara M, Akimitsu J, Eisaki H, Motoyama N and Uchida S 1998 *Phys. Rev. Lett.* **81** 1702
[10] Eccleston R S, Azuma M and Takano M 1996 *Phys. Rev.* B **53** R14721
[11] Kumagai K, Tsuji S, Kato M and Koike Y 1997 *Phys. Rev. Lett.* **78** 1992
[12] Lin C, Chen H and Wang Q 2001 *Phys. Rev.* B **64** 104517
[13] Yoshimitsu H, Hiroi M and Kawakami M 2003 *Physica* B **329–333** 1016
[14] Xie H, Hu N, Wang L, Lin Y, Xiong R, Yu Z, Tang W, Wang Q and Shi J 2006 *Physica* B **381** 168
[15] Wu X J, Takayama-Muromachi E and Horiuchi S 1991 *Acta Crystallogr.* A **47** 727
[16] Wang J, Zou H, Li Y and Shi J 2009 in preparation
[17] Tanaka M and Terauchi M 1985 *Convergent-Beam Electron Diffraction* (Tokyo: JEOL LTD)
[18] Hahn T 1983 *International Tables for Crystallography* vol A (Dordrecht: Reidel)
[19] Wang J, Zou H, Guo C, Wang L, Hu N and Shi J 2007 *J. Phys.: Condens. Matter* **19** 196224
[20] Matsuda M and Katsumata K 1996 *Phys. Rev.* B **53** 12201
[21] Azuma M, Hiroi Z, Takano M, Ishida K and Kitaoka Y 1994 *Phys. Rev. Lett.* **73** 3463
[22] Lin Y, Xiong R, Hu N, Wang L, Yu Z, Tang W and Shi J 2007 *Physica* B **400** 93
[23] Takigawa M, Motoyama N, Eisaki H and Uchida S 1998 *Phys. Rev.* B **57** 1124
[24] Wang Q, Lin C, Ni Y and Zhang Y 1999 *J. Appl. Phys.* **85** 6061
[25] Hatfield W E 1981 *J. Appl. Phys.* **52** 1985
[26] Hall J W, Marsh W E, Weller R R and Hatfield W E 1981 *Inorg. Chem.* **20** 1033
[27] Matsuda M, Katsumata K, Osafune T, Motoyama N, Eisaki H, Uchida S, Yokoo T, Shapiro S M, Shirane G and Zarestky J L 1997 *Phys. Rev.* B **56** 14499
[28] Kudo K, Ishikawa S, Noji T, Adachi T, Koike Y, Maki K, Tsuji S and Kumagai K 2000 *Physica* B **284–288** 651
[29] Adachi T, Shiota K, Kato M, Noji T and Koike Y 1998 *Solid State Commun.* **105** 639
[30] Motoyama N, Osafune T, Kakeshita T, Eisaki H and Uchida S 1997 *Phys. Rev.* B **55** R3386
[31] Eisaki H, Motoyama N, Kojima K M, Uchida S, Takeshita N and Mori N 2000 *Physica* C **341–348** 363
[32] Abrashev M V, Hadjimitov V N, Dinolova E and Bozukov L N 1993 *Physica* C **215** 421
[33] Abrashev M V, Thomsen C and Surtchev M 1997 *Physica* C **280** 297
[34] Osada M, Kakihana M, Nagai I, Noji T, Adachi T, Koike Y, Bäckström J, Käll M and Börjesson L 2000 *Physica* C **338** 161
[35] Kakihana M, Osada M, Käll M, Börjesson L, Mazaki H, Yasuoka H, Yashima M and Yoshimura M 1996 *Phys. Rev.* B **53** 11796